
UNCERTAINTY QUANTIFICATION FOR DISTRIBUTION-TO-DISTRIBUTION FLOW MATCHING IN SCIENTIFIC IMAGING

A PREPRINT

Dongxia Wu
Stanford University
Stanford, CA
dowu@stanford.edu

Yuhui Zhang
Stanford University
Stanford, CA
yuhuiz@stanford.edu

Serena Yeung-Levy
Stanford University
Stanford, CA
syyeung@stanford.edu

Emma Lundberg
Stanford University
Stanford, CA
emmalu@stanford.edu

Emily B. Fox
Stanford University
Stanford, CA
ebfox@stanford.edu

ABSTRACT

Distribution-to-distribution generative models support scientific imaging tasks ranging from modeling cellular perturbation responses to translating medical images across conditions. Trustworthy generation requires both *reliability* (generalization across labs, devices, and experimental conditions) and *accountability* (detecting out-of-distribution cases where predictions may be unreliable). Uncertainty quantification (UQ) based approaches serve as promising candidates for these tasks, yet UQ for distribution-to-distribution generative models remains underexplored. We present a unified UQ framework, Bayesian Stochastic Flow Matching (BSFM), that disentangles aleatoric and epistemic uncertainty. The Stochastic Flow Matching (SFM) component augments deterministic flows with a diffusion term to improve model generalization to unseen scenarios. For UQ, we develop a scalable Bayesian approach—MCD-Antithetic—that combines Monte Carlo Dropout with sample-efficient antithetic sampling to produce effective anomaly scores for out-of-distribution detection. Experiments on cellular imaging (BBBC021, JUMP) and brain fMRI (Theory of Mind) across diverse scenarios show that SFM improves reliability while MCD-Antithetic enhances accountability.

1 Introduction

Distribution-to-distribution generative image models have emerged as powerful tools across scientific domains, ranging from predicting cellular morphology changes under chemical and genetic perturbations [52] to mapping between resting-state and task-evoked brain activity in neuroimaging [31, 26], to translating medical images between control and treatment conditions [32, 3]. By learning transformations between well-defined source and target distributions, these models capture meaningful scientific relationships—how biological systems respond to interventions, how neural activity patterns shift across cognitive states, or how pathological conditions manifest in medical imaging. This makes them particularly valuable for biomedical imaging, where interpreting distributional transformations is central to the underlying scientific question.

Despite the potential of these models, deploying them in real-world scientific applications demands trustworthiness beyond mere generative quality [24, 6]. Trustworthiness in this context requires two complementary properties: **reliability**—the ability to generalize across distribution shifts such as different laboratories, imaging devices, or experimental protocols; and **accountability**—the capacity to detect out-of-distribution (OOD) scenarios and inform domain experts when predictions fall outside the model’s reliable operating range. Without these properties, models risk producing misleading predictions that could lead to costly experimental validation of false hypotheses, patient

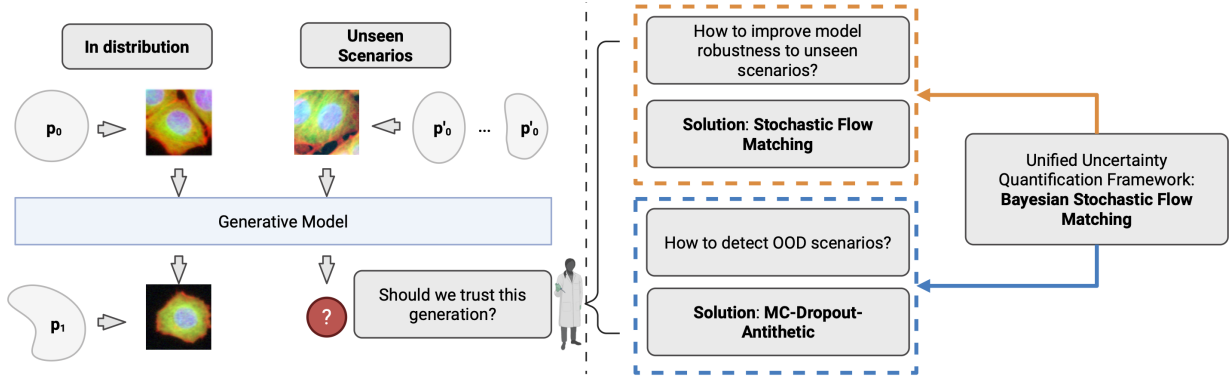


Figure 1: Trustworthy distribution-to-distribution generative modeling. **Left:** In-domain samples are drawn from the source distribution p_0 , while unseen samples may arise from shifted source distributions $\{p'_0\}$. **Right:** Our unified UQ framework, Bayesian Stochastic Flow Matching (BSFM), including Stochastic Flow Matching (SFM) to improve model generalizability, and MCD-Antithetic to efficiently and accurately estimate epistemic and aleatoric uncertainty for OOD detection.

safety concerns, or missed scientific opportunities. For instance, in drug discovery, a cellular morphology prediction model that confidently predicts responses to novel compounds without flagging uncertainty could misdirect expensive screening campaigns. Fig. 1 (left) illustrates the challenges we aim to address.

Uncertainty quantification (UQ) offers a promising approach to address such aspects of model trustworthiness. However, to the best of our knowledge, UQ for distribution-to-distribution generative models remains unexplored—a critical gap for deploying these models in practice. Performing UQ on distribution-to-distribution generative models requires solving several technical challenges. First, state-of-the-art distribution-to-distribution models like flow matching [34, 52] are deterministic, producing a single output for each input without capturing uncertainty in the transformation process. This limits their ability to quantify both aleatoric uncertainty (inherent variability in the data-generating process) and epistemic uncertainty (model uncertainty from limited data and model misspecification). Second, existing UQ methods face challenges in scaling to high-dimensional image-based generative models. For example, deep ensembles are often computationally expensive, and variational inference based methods can become intractable in high-dimensional parameter spaces. Naive sampling-based approaches are typically sample-inefficient, requiring many forward passes for stable uncertainty estimates.

Building on flow matching, which learns continuous transformations via neural ordinary differential equations (ODEs), we develop Bayesian Stochastic Flow Matching (BSFM) to quantify aleatoric and epistemic uncertainty in a unified framework. We first extend deterministic flow matching to stochastic flow matching (SFM) by introducing a learnable diffusion term while preserving the learned marginals, capturing inherent data variability as aleatoric uncertainty. We further propose a scalable Bayesian treatment of SFM—MCD-Antithetic—using Monte Carlo Dropout to approximate the model posterior. Via nested sampling, we decompose total uncertainty into aleatoric and epistemic components, and use antithetic sampling to improve sample efficiency. The resulting MCD-Antithetic uncertainty terms provide effective anomaly scores for OOD detection without architectural changes and additional training. Additionally, our uncertainty decomposition provides enhanced explainability of OOD detections.

Through extensive experiments on cellular imaging datasets (BBBC021, JUMP) and an fMRI dataset (‘Theory of Mind’, ToM) across diverse unseen scenarios—novel perturbations, different laboratory settings, novel cell lines, unseen plates, and low-performing ToM subjects—we demonstrate the effectiveness of SFM and MCD-Antithetic. Specifically, SFM improves model reliability through enhanced generalization under distribution shifts, while MCD-Antithetic quantifies epistemic uncertainty and aleatoric uncertainty in a sample-efficient way to provide effective and interpretable OOD detection signals. Jointly, our framework establishes a principled recipe for building trustworthy distribution-to-distribution generative models in scientific applications, see Fig. 1 (right). In summary, our contributions are:

- We present a unified uncertainty quantification framework **Bayesian Stochastic Flow Matching (BSFM)** for distribution-to-distribution generative models that enables principled decomposition into aleatoric and epistemic components.
- Our **Stochastic Flow Matching (SFM)** explicitly captures aleatoric uncertainty to enhance generalization under distributional shifts.

- Our **MCD-Antithetic** technique provides a sample-efficient approach to estimate epistemic and aleatoric uncertainty, supporting effective OOD detection.
- Our extensive experiments demonstrate that our approach improves both **reliability** and **accountability**.

2 Related Work

Distribution-to-distribution Generative Models. Distribution-to-Distribution generative models learn mappings between two well-defined data distributions, in contrast to conventional noise-to-data generation. This paradigm has found applications across diverse scientific domains [52, 31, 26, 32, 3]. These models are typically built upon flow-based architectures [34, 35], diffusion bridge models [43, 54, 11], or variants of generative adversarial networks [55, 41, 27]. Flow matching has emerged as a particularly promising approach due to its efficient training via regression on velocity fields and straightforward inference through ordinary differential equation (ODE) integration. Recent extensions include classifier-free guidance for enhanced conditional generation [52] and stochastic injections to improve in-distribution performance [46]. While these models achieve impressive image generation fidelity on in-distribution data, their behavior under distribution shifts remains largely unexplored, motivating the need to build a UQ-based framework to address these challenges.

Uncertainty Quantification in Generative Models. UQ in generative models has gained growing interest, especially for diffusion models. For epistemic uncertainty, Bayesian formulations such as BayesDiff [30] and Jazbec et al. [25] adopt last-layer Laplace approximations in a post-hoc manner, while ensemble-based approaches like DECU [5] capture model variability through multiple denoisers. For aleatoric uncertainty, diffusion models naturally support posterior sampling to quantify data variability [12]. Applications include inverse imaging methods [49, 14, 48] and text-to-image generation [15], with conformal prediction approaches [47, 13] providing distribution-free coverage guarantees. Hyper-Diffusion [8] decomposes both uncertainty types within a single hypernetwork model but requires computationally expensive nested sampling. However, existing UQ methods primarily target *noise-to-data* generation using *diffusion models*, while UQ for *flow-based models* in *distribution-to-distribution* settings remains unexplored.

Out-of-Distribution Detection in Generative Models. OOD detection in generative models has been widely studied, primarily using reconstruction or manifold consistency approaches. Methods include diffusion inpainting for manifold projection [37], denoising trajectory analysis [19], semantic mismatch measurement [18], and projection regret [10]. Geometric and statistical cues such as diffusion-path curvature [22], covariance spectra [44], and norm-guided residuals [50] have also been explored. Applications span medical imaging [20, 4, 33], road-scene analysis [17], and zero-shot [1] or trend-based [28] anomaly detection. However, these methods operate in noise-to-data or image-to-manifold regimes, defining OOD globally with respect to a single data distribution. In contrast, our work addresses distribution-to-distribution settings where the definition of OOD is conditional on the source distribution—a source-aware regime has not been addressed by existing diffusion or flow-matching approaches.

3 Preliminaries

3.1 Distribution-to-Distribution Image Generation

Let \mathcal{X} denote the image space. Let p_0 be a source distribution and p_1 a target distribution over \mathcal{X} . The goal of distribution-to-distribution image generation is to learn a generative model mapping p_0 to p_1 . Given an image $\mathbf{x}_0 \sim p_0$, generate $\mathbf{x}_1 \sim p_1$ that represents the transformed image in the target distribution. Optionally, we can incorporate a condition space \mathcal{C} to enable conditional generation, where the target distribution becomes $p_1(\cdot|c)$ for $c \in \mathcal{C}$. In this case, we learn a conditional generative model $p(\mathbf{x}_1|\mathbf{x}_0, c)$ that maps $\mathbf{x}_0 \sim p_0$ to $\mathbf{x}_1 \sim p_1(\cdot|c)$. For instance, in cellular imaging, p_0 represents the distribution of unperturbed cell images, $p_1(\cdot|c)$ represents the distribution of cell images under drug perturbation c , and the model predicts morphological changes induced by the perturbation.

3.2 Flow Matching-based Generative Modeling

Flow matching-based generative models learn invertible mappings between p_0 and p_1 via continuous transformations. Given pairs of samples from these distributions, flow matching learns a time-dependent velocity field using a neural network $\mathbf{v}_\theta : \mathcal{X} \times [0, 1] \rightarrow \mathcal{X}$ that defines the instantaneous direction and magnitude of change at each point. The transformation process follows the ODE:

$$\frac{d\mathbf{x}_t}{dt} = \mathbf{v}_\theta(\mathbf{x}_t, t), \quad \mathbf{x}_0 \sim p_0, \mathbf{x}_1 \sim p_1, t \in [0, 1]. \quad (1)$$

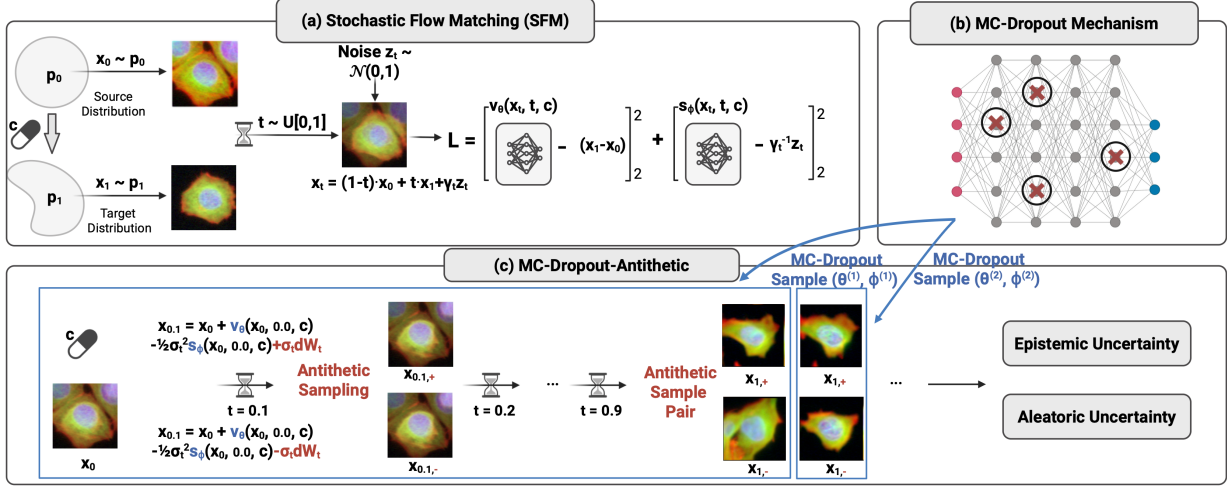


Figure 2: Core components of the Bayesian Stochastic Flow Matching (BSFM) framework: (a) Stochastic flow matching (SFM) training process. (b) MC-Dropout mechanism applied to the U-Net architecture of the SFM model. (c) MCD-Antithetic nested sampling.

We follow [36] to employ the rectified flow formulation which yields a straight-line path:

$$\mathbf{x}_t = (1-t)\mathbf{x}_0 + t\mathbf{x}_1, \quad t \sim \mathcal{U}[0, 1]. \quad (2)$$

The linear path has constant velocity field $\mathbf{v}(\mathbf{x}_t, t) = d\mathbf{x}_t/dt = \mathbf{x}_1 - \mathbf{x}_0$, which represents the optimal transport direction at each point. The neural network \mathbf{v}_θ is trained to match this velocity field by minimizing:

$$\mathcal{L}(\theta) = \mathbb{E}_{(\mathbf{x}_0, \mathbf{x}_1) \sim p_0 \times p_1, t \sim \mathcal{U}(0,1)} \|\mathbf{v}_\theta(\mathbf{x}_t, t) - (\mathbf{x}_1 - \mathbf{x}_0)\|_2^2. \quad (3)$$

At inference, given input $\mathbf{x}_0 \sim p_0$, we solve the ODE from $t = 0$ to $t = 1$ to obtain the deterministic output $\hat{\mathbf{x}}_1$:

$$\hat{\mathbf{x}}_1 = \mathbf{x}_0 + \int_0^1 \mathbf{v}_\theta(\mathbf{x}_t, t) dt. \quad (4)$$

3.3 Conditional Flow Matching

To model $p(\mathbf{x}_1|\mathbf{x}_0, c)$, we follow [52] to extend flow matching to conditional flow matching (CFM) for condition $c \in \mathcal{C}$. The source distribution $p_0(\mathbf{x})$ represents images in a reference state, while the target distribution $p_1(\mathbf{x}|c)$ captures condition-dependent changes. CFM learns a conditional vector field $\mathbf{v}_\theta : \mathcal{X} \times [0, 1] \times \mathcal{C} \rightarrow \mathcal{X}$ defining the flow from p_0 to $p_1(\cdot|c)$ via ODE:

$$\frac{d\mathbf{x}_t}{dt} = \mathbf{v}_\theta(\mathbf{x}_t, t, c), \quad \mathbf{x}_0 \sim p_0, \mathbf{x}_1 \sim p_1(\cdot|c). \quad (5)$$

We apply classifier-free guidance [23, 53] to enhance conditional generation. During training, we randomly mask condition c with probability p_c , replacing it with null condition c_\emptyset . At inference, conditional and unconditional predictions combine to form the guided vector field:

$$\tilde{\mathbf{v}}_\theta(\mathbf{x}_t, t, c) = \alpha \mathbf{v}_\theta(\mathbf{x}_t, t, c) + (1-\alpha) \mathbf{v}_\theta(\mathbf{x}_t, t, c_\emptyset), \quad (6)$$

where $\alpha \geq 1$ controls the guidance strength.

Henceforth, we use the conditional notation $p(\mathbf{x}_1|\mathbf{x}_0, c)$ and $p_1(\cdot|c)$ as a unified representation for both conditional and unconditional cases. The unconditional case can be recovered via $c = c_\emptyset$.

4 Methodology

We develop a UQ framework, **BSFM**, that stochastically maps inputs \mathbf{x}_0 to outputs $\hat{\mathbf{x}}_1$ conditioned on c and accounts for parameter uncertainty. BSFM enables decomposing predictive variance—our UQ measure—into epistemic and aleatoric components. We propose **MCD-Antithetic** for computationally-tractable estimation of these quantities via nested sampling leveraging the scalability of MC-Dropout and the sample-efficiency of antithetic sampling. See Fig. 2 for each of the components of **BSFM**.

4.1 Stochastic Flow Matching

To quantify the aleatoric uncertainty inherent to the transformation process, a naive extension adds diffusion noise to the ODE solver of the learned velocity field:

$$d\mathbf{x}_t = \mathbf{v}_\theta(\mathbf{x}_t, t, c)dt + \sigma_t d\mathbf{W}_t, \quad (7)$$

where σ_t is a predefined noise schedule and \mathbf{W}_t denotes standard Brownian motion. However, this directly perturbs the marginals $p_t(\mathbf{x}_t|c)$ at each time t , deviating from the learned transport and degrading generation quality. We instead derive a marginal-preserving stochastic differential equation (SDE) via the Fokker-Planck equation [45]. For any ODE $d\mathbf{x}_t = \mathbf{v}_\theta(\mathbf{x}_t, t, c)dt$ with marginals $\{p_t(\mathbf{x}_t|c)\}$, the corresponding SDE with drift correction:

$$d\mathbf{x}_t = \left(\mathbf{v}_\theta(\mathbf{x}_t, t, c) - \frac{1}{2}\sigma_t^2 \nabla_{\mathbf{x}_t} \log p_t(\mathbf{x}_t|c) \right) dt + \sigma_t d\mathbf{W}_t \quad (8)$$

shares identical marginals $p_t(\mathbf{x}_t|c)$ for all $t \in [0, 1]$. The score correction term compensates for diffusion-induced drift, preserving the learned distribution-to-distribution mapping while introducing controlled stochasticity.

Training and Inference. We parameterize the score function as $s_\phi(\mathbf{x}_t, t, c) \approx \nabla_{\mathbf{x}_t} \log p_t(\mathbf{x}_t|c)$ and train it jointly with the velocity field. Following [2], we perturb the interpolation path of the standard score matching model:

$$\mathbf{x}_t = (1-t)\mathbf{x}_0 + t\mathbf{x}_1 + \gamma_t \mathbf{z}_t, \quad \mathbf{z}_t \sim \mathcal{N}(\mathbf{0}, \mathbf{I}), \quad (9)$$

where γ_t is a smooth noise schedule with $\gamma_0 = \gamma_1 = 0$. For $\gamma_t > 0$, the score admits the analytic form $\nabla_{\mathbf{x}_t} \log p_t(\mathbf{x}_t|c) = -\gamma_t^{-1} \mathbf{z}_t$. We set $\gamma_t = a \sin^2(\pi t)$ and minimize the combined objective:

$$\mathcal{L}_v(\theta) = \mathbb{E} \|\mathbf{v}_\theta(\mathbf{x}_t, t, c) - (\mathbf{x}_1 - \mathbf{x}_0)\|_2^2, \quad (10)$$

$$\mathcal{L}_s(\phi) = \mathbb{E} \|s_\phi(\mathbf{x}_t, t, c) + \gamma_t^{-1} \mathbf{z}_t\|_2^2, \quad (11)$$

$$\mathcal{L}(\theta, \phi) = \mathcal{L}_v(\theta) + \lambda \mathcal{L}_s(\phi), \quad (12)$$

where expectations are taken over $(\mathbf{x}_0, \mathbf{x}_1) \sim p_0 \times p_1(\cdot|c)$ and $t \sim \mathcal{U}(0, 1)$. At inference, we solve the SDE using the learned velocity and score networks to generate samples:

$$d\mathbf{x}_t = \left(\mathbf{v}_\theta(\mathbf{x}_t, t, c) - \frac{1}{2}\sigma_t^2 s_\phi(\mathbf{x}_t, t, c) \right) dt + \sigma_t d\mathbf{W}_t. \quad (13)$$

4.2 Bayesian Stochastic Flow Matching

To quantify epistemic uncertainty, we adopt a Bayesian treatment of the velocity and score network parameters (θ, ϕ) . Given training data \mathcal{D} , the posterior is given by:

$$p(\theta, \phi|\mathcal{D}) \propto p(\mathcal{D}|\theta, \phi)p(\theta, \phi), \quad (14)$$

where $p(\mathcal{D}|\theta, \phi)$ denotes the likelihood and $p(\theta, \phi)$ the prior. The predictive distribution marginalizes over parameter uncertainty:

$$p(\mathbf{x}_1|\mathbf{x}_0, c, \mathcal{D}) = \iint p(\mathbf{x}_1|\mathbf{x}_0, c, \theta, \phi)p(\theta, \phi|\mathcal{D})d\theta d\phi, \quad (15)$$

where $p(\mathbf{x}_1|\mathbf{x}_0, c, \theta, \phi)$ is the conditional distribution induced by the SDE in Eq. equation 13.

4.3 Uncertainty Decomposition and Estimation

Total predictive uncertainty arises from two sources: aleatoric uncertainty, reflecting inherent stochasticity in the transformation captured by $p(\mathbf{x}_1|\mathbf{x}_0, c, \theta, \phi)$, and epistemic uncertainty, arising from limited training data and captured by the model posterior $p(\theta, \phi|\mathcal{D})$.

We quantify uncertainty via variance and decompose total predictive variance using the law of total variance:

$$\text{Var}(\mathbf{x}_1|\mathbf{x}_0, c, \mathcal{D}) = \underbrace{\mathbb{E}_{p(\theta, \phi|\mathcal{D})}[\text{Var}(\mathbf{x}_1|\mathbf{x}_0, c, \theta, \phi)]}_{\text{aleatoric uncertainty}} + \underbrace{\text{Var}_{p(\theta, \phi|\mathcal{D})}[\mathbb{E}(\mathbf{x}_1|\mathbf{x}_0, c, \theta, \phi)]}_{\text{epistemic uncertainty}}, \quad (16)$$

where the first term represents aleatoric uncertainty and the second term represents epistemic uncertainty.

We employ nested sampling to estimate both uncertainty terms: for each of M posterior parameter samples $(\theta^{(m)}, \phi^{(m)}) \sim p(\theta, \phi | \mathcal{D})$, we solve the SDE K times generating $\mathbf{x}_1^{(k,m)} \sim p(\cdot | \mathbf{x}_0, c, \theta^{(m)}, \phi^{(m)})$, and estimate:

$$\hat{\mu}^{(m)} = \frac{1}{K} \sum_{k=1}^K \mathbf{x}_1^{(k,m)} \approx \mathbb{E}(\mathbf{x}_1 | \mathbf{x}_0, c, \theta^{(m)}, \phi^{(m)}), \quad (17)$$

and

$$\hat{\Sigma}^{(m)} = \frac{1}{K-1} \sum_{k=1}^K (\mathbf{x}_1^{(k,m)} - \hat{\mu}^{(m)})(\mathbf{x}_1^{(k,m)} - \hat{\mu}^{(m)})^T \approx \text{Var}(\mathbf{x}_1 | \mathbf{x}_0, c, \theta^{(m)}, \phi^{(m)}). \quad (18)$$

For our estimate of aleatoric uncertainty, we compute:

$$\hat{A} = \frac{1}{M} \sum_{m=1}^M \hat{\Sigma}^{(m)} \quad (19)$$

For epistemic uncertainty, we note that by the law of total variance (conditioning on \mathbf{x}_0, c),

$$\text{Var}_{p(\theta, \phi | \mathcal{D})}[\hat{\mu}(\theta, \phi)] = \underbrace{\text{Var}_{p(\theta, \phi | \mathcal{D})}[\mathbb{E}(\hat{\mu} | \theta, \phi)]}_{\text{epistemic uncertainty}} + \underbrace{\mathbb{E}_{p(\theta, \phi | \mathcal{D})}[\text{Var}(\hat{\mu} | \theta, \phi)]}_{\text{residual Monte Carlo noise}}. \quad (20)$$

The first term equates with true epistemic uncertainty because $\mathbb{E}(\hat{\mu} | \theta, \phi) = \mathbb{E}(\mathbf{x}_1 | \mathbf{x}_0, c, \theta, \phi)$. Additionally, note that $\text{Var}(\hat{\mu} | \theta, \phi) = \frac{1}{K} \text{Var}(\mathbf{x}_1 | \mathbf{x}_0, c, \theta, \phi)$. That is, the residual Monte Carlo (MC) noise is aleatoric uncertainty corruption, scaled by the sample size K , that shows up in the naive estimator for epistemic uncertainty:

$$\hat{E} = \frac{1}{M-1} \sum_{m=1}^M (\hat{\mu}^{(m)} - \bar{\mu})(\hat{\mu}^{(m)} - \bar{\mu})^T. \quad (21)$$

Ideally, we would correct for this MC noise by subtracting \hat{A}/K . However, nested sampling incurs $\mathcal{O}(M \times K)$ SDE solves, which is computationally prohibitive for high-dimensional images for large M, K , the regime where our estimates are lower variance. To handle this, we introduce an alternative sample-efficient method.

4.4 Scalable and Sample-Efficient Uncertainty Estimation

Estimating the Model Posterior $p(\theta, \phi | \mathcal{D})$. Exact Bayesian inference for deep neural networks is typically intractable. We therefore adopt MC-Dropout, a scalable approach to approximate the posterior [16]. As shown in Fig. 2, we insert dropout layers in the velocity and score networks. At inference, we keep dropout active and perform multiple stochastic forward passes, yielding samples $\{(\theta^{(m)}, \phi^{(m)})\}_{m=1}^M$ from the approximate posterior. This provides a simple and scalable method in high-dimensional parameter spaces.

MCD-Antithetic The conditional distribution $p(\mathbf{x}_1 | \mathbf{x}_0, c, \theta, \phi)$ is defined by our proposed SFM SDE, where stochasticity arises from the driving Brownian motion. Accurate estimation of the moments required for uncertainty decomposition typically necessitates aggregating many SDE trajectories, which is computationally expensive. To alleviate this cost, we employ antithetic sampling [21] to reduce MC variance while using a limited number of samples. Specifically, for each noise realization ϵ used to drive the SDE, we additionally simulate the trajectory induced by its negation $-\epsilon$. This construction introduces negative correlation between paired samples, thereby reducing estimator variance without bias under the usual symmetry of the driving noise.

In particular, for J antithetic pairs ($K = 2J$ total samples), $(\mathbf{x}_{1,+}^{(j,m)}, \mathbf{x}_{1,-}^{(j,m)})$, we form

$$\mathbf{y}^{(j,m)} = \frac{1}{2}(\mathbf{x}_{1,+}^{(j,m)} + \mathbf{x}_{1,-}^{(j,m)}), \quad \hat{\mu}_{anti}^{(m)} = \frac{1}{J} \sum_{j=1}^J \mathbf{y}^{(j,m)}. \quad (22)$$

We use $\hat{\mu}_{anti}^{(m)}$ to produce reduced variance estimates of both aleatoric and epistemic uncertainty, \hat{A} and \hat{E} , respectively. Importantly, antithetic sampling reduces the residual MC error in Eq. equation 20 by effectively increasing our sample size K , enabling more reliable epistemic uncertainty estimation under tight computational budgets. See Fig. 2.

Method	BBBC021				JUMP				fMRI	
	Unseen Pert.		Intensity Shift		Unseen Cell Lines		Unseen Plates		Low ToM	
	FID↓	KID↓	FID↓	KID↓	FID↓	KID↓	FID↓	KID↓	FID↓	KID↓
UNSB	88.31	6.27	56.95	4.7	57.24	4.19	45.5	4.04	75.54	8.89
SDEdit	<u>37.18</u>	3.48	<u>29.57</u>	2.72	33.96	3.11	13.21	0.9	56.87	6.15
CellFlux	103.73	12.76	62.01	5.84	<u>39.06</u>	3.4	<u>17.81</u>	<u>1.04</u>	<u>34.86</u>	<u>2.63</u>
SFM	33.29	2.02	28.14	1.87	25.1	1.75	18.02	1.23	25.55	1.47

Table 1: Generalization performance on unseen scenarios. We report FID and KID scores (lower is better) across 5 OOD scenarios on BBBC021, JUMP, and fMRI datasets. Best results are in **bold**, second best are underlined.

MAP Approximation for Aleatoric Uncertainty. For aleatoric uncertainty estimation, we can approximate the expectation using only the MAP estimate $(\hat{\theta}, \hat{\phi})$, reducing the cost to $\mathcal{O}(K)$ SDE solves. This is justified when the posterior is concentrated and the conditional variance is smooth in the parameters, as formalized below.

Proposition 4.1 (MAP Approximation for Aleatoric Uncertainty). *Let $V(\theta, \phi) := \text{Var}(\mathbf{x}_1 | \mathbf{x}_0, c, \theta, \phi)$. If V is L -Lipschitz continuous in (θ, ϕ) and $p(\theta, \phi | \mathcal{D}) \approx \mathcal{N}((\hat{\theta}, \hat{\phi}), \mathbf{H}^{-1})$ with $\|\mathbf{H}^{-1}\|_{op} \leq \epsilon^2$, then*

$$\left| \mathbb{E}_{p(\theta, \phi | \mathcal{D})}[V(\theta, \phi)] - V(\hat{\theta}, \hat{\phi}) \right| \leq L\epsilon\sqrt{d}, \quad (23)$$

where $d = \dim(\theta, \phi)$.

The proof is provided in Appendix A.

5 Results

We assess BSFM’s effectiveness on generalization and OOD detection tasks within cellular and fMRI imaging and compare to a number of baseline alternative approaches.

5.1 Datasets

We evaluate on two cell-imaging benchmarks: **BBBC021** (chemical perturbations) [7] and **JUMP** (chemical and genetic perturbations) [9]. To probe robustness and OOD detection, we define four scenarios spanning mild to severe distribution shifts: **Unseen Plates** and **Unseen Cell Lines** in JUMP, synthetic **Intensity Shift** in BBBC021 to mimic imaging-condition variation across different laboratory settings, and a combined **Unseen Pert.** setting with unseen perturbations and intensity shifts. We further evaluate **Intensity Shift** scenarios in JUMP for OOD detection, spanning a full range of distribution shifts from mild to severe. To evaluate generalization to unseen data, we additionally assess performance on an **fMRI** Theory-of-Mind (ToM) dataset [42], where the objective is to transform resting-state scans to task-activated states. We train on high-performing ToM subjects and evaluate generalization to low-performing (LToM) subjects. Table 4 summarizes datasets and scenarios. More details are provided in Appendix B.

5.2 Experimental Setup

Baselines. For generalization, we compare **SFM** against: **CellFlux** [52], a state-of-the-art deterministic flow matching model for distribution-to-distribution cell image generation; **UNSB** [27], which employs a multi-step GAN to learn a Schrödinger bridge between source and target distributions; and **SDEdit** [39], which performs partial noising of the source sample followed by denoising to generate the target sample. For OOD detection, we establish a benchmark by comparing different UQ approaches within the distribution-to-distribution flow matching framework. We compare **MCD-Antithetic** to: **Transform Distance (TransDist)**, a non-uncertainty-based baseline that uses the distance between the generated and source images as the anomaly score; **MAP**, which captures aleatoric uncertainty; and **Laplace Approximation (LA)** [30] and **Stochastic Weight Averaging-Gaussian (SWAG)** [38], both of which we use as alternatives to MC Dropout in quantifying aleatoric and epistemic uncertainty via nested sampling. All baselines are adapted to the SFM setting to enable fair comparison.

Training and evaluation details. We evaluate generation quality using Fréchet Inception Distance (FID) and Kernel Inception Distance (KID) to measure distribution similarity. For OOD detection, we report area under the receiver operating characteristic curve (AUROC) and area under the precision-recall curve (AUPR). To create ground truth

Method	BBBC021				JUMP					
	Unseen Pert.		Intensity Shift		Unseen Cell Lines		Unseen Plates		Intensity Shift	
	AUROC↑	AUPR↑	AUROC↑	AUPR↑	AUROC↑	AUPR↑	AUROC↑	AUPR↑	AUROC↑	AUPR↑
TransDist	0.6208	0.3223	0.621	0.4803	0.6193	0.5419	0.5105	0.5233	0.683	0.5282
MAP Aleatoric	0.6676	0.4375	0.6979	0.6201	0.7841	0.7293	0.6968	0.6146	0.3256	0.3366
SWAG Aleatoric	0.6397	0.4255	0.5906	0.5735	0.8595	0.8303	0.7268	0.6663	0.3545	0.3464
SWAG Epistemic	0.6849	0.5424	0.6678	0.6923	0.8251	0.7627	0.6954	0.6186	0.8997	0.8265
LA Aleatoric	0.6349	0.4461	0.5772	0.5671	0.8561	0.8242	0.741	0.6721	0.3224	0.3359
LA Epistemic	0.6538	0.4583	0.6353	0.6455	0.8003	0.7486	0.7046	0.6327	0.5727	0.4682
MCD-Independent Aleatoric	0.7395	0.4853	0.7218	0.6467	0.8586	0.8239	0.7359	0.6549	0.4426	0.3783
MCD-Independent Epistemic	0.7373	0.4881	0.7481	0.659	0.8417	0.8074	0.7279	0.6571	0.4322	0.3739
MCD-Antithetic Aleatoric	0.7304	0.5001	0.709	0.6433	0.8696	0.8428	0.7444	0.6762	0.3568	0.347
MCD-Antithetic Epistemic	0.8071	0.6718	0.7698	0.7505	0.8034	0.7454	0.6792	0.5988	0.9063	0.8311

Table 2: Out-of-Distribution detection performance. We report AUROC and F1 scores (higher is better) across 5 OOD scenarios on BBBC021 and JUMP datasets. Both the SWAG and LA baselines use antithetic sampling for fair comparison. The table groups methods into baselines, ablation studies evaluating antithetic sampling, and MCD-Antithetic, separated by horizontal rules. Best results are in **bold**.

Method	BBBC021				JUMP					
	Unseen Pert.		Intensity Shift		Unseen Cell Lines		Unseen Plates		Intensity Shift	
	AUROC↑	AUPR↑	AUROC↑	AUPR↑	AUROC↑	AUPR↑	AUROC↑	AUPR↑	AUROC↑	AUPR↑
MCD-Independent Aleatoric	0.743	0.5149	0.7207	0.6523	0.8586	0.8239	0.7359	0.6549	0.4426	0.3783
MCD-Independent Epistemic	0.7151	0.5	0.7205	0.6469	0.8417	0.8074	0.7279	0.6571	0.4322	0.3739
MC-Dropout Epistemic (corrected) Independent	0.6143	0.3862	0.6403	0.5674	0.7825	0.7218	0.6654	0.5799	0.3837	0.3569
MCD-Antithetic Aleatoric	0.7247	0.4919	0.721	0.6433	0.8727	0.8419	0.748	0.6805	0.3923	0.3588
MCD-Antithetic Epistemic	0.7877	0.6513	0.7605	0.7291	0.8169	0.7587	0.5816	0.4984	0.9086	0.8363
MC-Dropout Epistemic (corrected) Antithetic	0.7557	0.5491	0.7087	0.6529	0.7319	0.6743	0.6258	0.5549	0.7821	0.6578

Table 3: Antithetic vs. independent sampling. We report AUROC and F1 scores (higher is better) across 5 OOD scenarios on BBBC021 and JUMP datasets. Best results are in **bold**.

OOD labels, we take all scenarios unseen during training and filter them to OOD samples as follows. First recall that our OOD detection task focuses on understanding for which p_0 we should not trust generations \mathbf{x}_1 . As we demonstrate in Sec. 5.3, our SFM enhances generalization implying that we may form reliable, ID-looking generations in some unseen scenarios. We aim to filter these samples as they do not represent true OOD scenarios. To this end, we filter samples using prediction error measured in the feature space of a mode-of-action pretrained classifier (BBBC021) [52] or in Structural Similarity Index Measure (SSIM) space (JUMP), and only flag high-error cases as OOD. Further details are in Appendix C.

For the uncertainty-based methods, we use $-tr(\hat{E})$ or $-tr(\hat{A})$ as the anomaly score, $f(\mathbf{x}_0, c)$, for epistemic and aleatoric, respectively. For TransDist, we use $f(\mathbf{x}_0, c) = \|\mathbf{x}_0 - \hat{\mathbf{x}}_1\|_2$. For MAP, we use the mean pixel-wise variance as the anomaly score. We then apply a binary decision rule:

$$h(\mathbf{x}_0, c) = \begin{cases} \text{OOD}, & \text{if } f(\mathbf{x}_0, c) > \tau \\ \text{ID}, & \text{if } f(\mathbf{x}_0, c) \leq \tau \end{cases} \quad (24)$$

where τ is a threshold parameter. Our choice of $-tr$ instead of tr is motivated by the well-documented fact that—seemingly counterintuitively—epistemic uncertainty for generative models *decreases* with increasingly large distribution shifts; this is due to model collapse leading to overconfidence OOD [29, 51]. Our epistemic uncertainty estimate still allows for detecting such OOD generations, but necessitates a sign flip. Similarly, we observe that aleatoric uncertainty decreases under distribution shift, exhibiting particular sensitivity to mild deviations; hence, we apply the same sign flip.

Following CellFlux [52], we adopt a U-Net based architecture to parameterize the velocity field. Perturbation conditions are encoded using IMPA [40]. We train models for 100 epochs on BBBC021, and 200 epochs on JUMP and fMRI using 2 NVIDIA H100 GPUs. For generation quality, we evaluate using 5000 generated images per unseen scenario on BBBC021 and JUMP, and 1024 images on fMRI. For OOD detection, we evaluate on randomly selected 500 ID and 500 OOD images per scenario (except 250 OOD images for Unseen Pert due to data availability). For MAP, we generate 2 antithetic pairs (4 total samples) per image. For MC-Dropout, LA, and SWAG, we generate 8×4 samples per image via nested sampling, where the 4 SDE samples arise from 2 antithetic pairs.

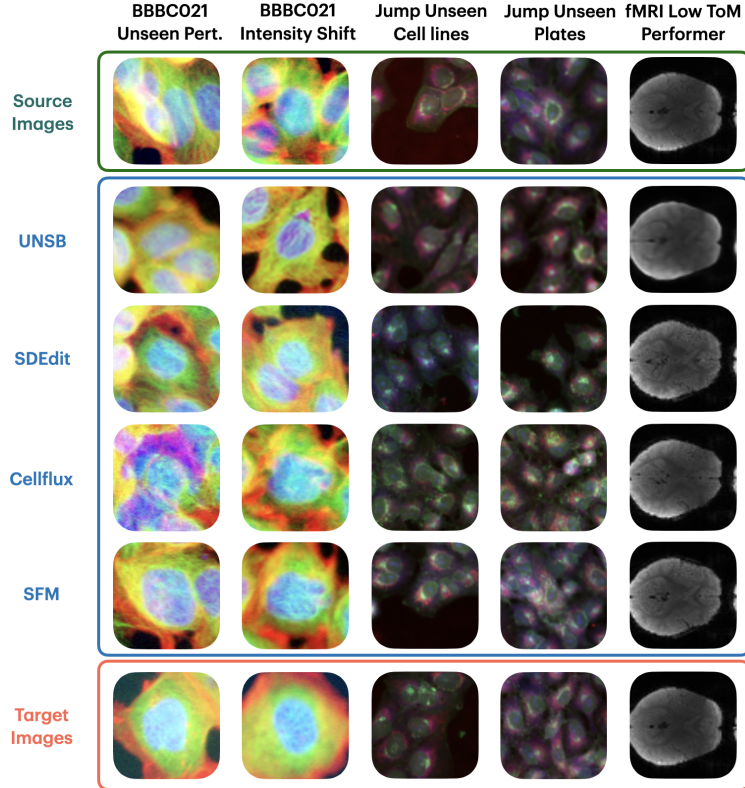


Figure 3: Examples of generated images from different methods under various unseen scenarios, compared with the source images and the ground truth target images.

5.3 Main Results

Stochastic Flow Matching Improves Generalization. Our proposed SFM demonstrates significant improvements in generalization across all unseen scenarios. As shown in Table 1, our method outperforms existing baselines, achieving consistent gains in both FID and KID metrics. The performance improvement is more apparent under the scenario with medium to severe distribution shifts, including unseen perturbations on BBBC021, intensity shifts on BBBC021, unseen cell lines on JUMP, and low Theory of Mind on fMRI. This overall improved robustness stems from explicitly modeling aleatoric uncertainty through stochastic perturbations during training and SDE-based sampling at inference. By capturing the inherent variability in the conditional distribution $p(\mathbf{x}_1 | \mathbf{x}_0, c, \theta, \phi)$ ¹ rather than learning a deterministic mapping, the model avoids overfitting to spurious correlations specific to the training distribution. The resulting uncertainty-aware generation process produces diverse, plausible outputs that better generalize to unseen distribution shifts. Examples of the generated images together with the corresponding source and ground truth target images are shown in Fig. 3.

OOD Detection Performance Analysis. As shown in Table 2, UQ-based methods consistently outperform the non-uncertainty baseline (TransDist) across all OOD scenarios, indicating that aleatoric and epistemic uncertainty provide informative signals for OOD detection. MAP, which captures only aleatoric uncertainty, yields moderate gains over TransDist. While it slightly underperforms nested-sampling UQ methods (SWAG, LA, MCD-Antithetic), it requires only 4 samples per image versus 32, offering a more computationally efficient alternative. Among SWAG, LA, and MCD-Antithetic, all using antithetic sampling, MCD-Antithetic achieves the strongest performance across all OOD scenarios, suggesting a more accurate and reliable uncertainty estimate in high-dimensional generative modeling. Finally, we observe a consistent pattern that epistemic uncertainty performs better on scenarios with severe distribution shifts (Unseen Pert., Intensity Shift), whereas aleatoric uncertainty performs better on slight distribution shifts (Unseen Cell Lines, Unseen Plates). This behavior is consistent with how different shift regimes affect the predictive decomposition. When inputs lie far outside the training support, posterior samples tend to extrapolate similarly under

¹One would imagine integrating over posterior uncertainty in (θ, ϕ) would further improve generalization; however, averaging image generations \mathbf{x}_1 pixel-wise reduces image quality.

shared inductive biases, which collapses model disagreement and shrinks epistemic uncertainty. By contrast, mild shifts largely preserve the learned mapping but reduce intrinsic conditional variability, so aleatoric uncertainty drops more rapidly. Overall, well-disentangled aleatoric and epistemic estimates provide complementary signals for OOD detection.

Ablation Study. One of the key issues that plagues UQ methods is that the estimated epistemic and aleatoric uncertainty are highly entangled, making it hard to utilize their complementary information for OOD detection. Antithetic sampling is a simple yet effective variance reduction technique that can help de-correlate the two uncertainty estimates in our MCD-Antithetic framework. To evaluate the effect of antithetic sampling in MC-Dropout, we compare it to MCD-Independent using independent sampling in Table 2. For independent sampling, we generate 4 samples per image; for antithetic sampling, we generate 2 paired samples per image. We observe that the aleatoric and epistemic estimates are highly correlated under independent sampling, suggesting that the epistemic signal is substantially contaminated by aleatoric variability. Antithetic sampling mitigates this coupling, better disentangling the two uncertainty components, and improving OOD detection performance.

6 Conclusion

We presented a systematic study of uncertainty quantification for trustworthy distribution-to-distribution generative modeling in scientific imaging. Building on flow matching, we introduced Bayesian Stochastic Flow Matching (BSFM), which unifies aleatoric and epistemic uncertainty in a single framework. On the reliability side, we proposed Stochastic Flow Matching (SFM), extending deterministic flows with a learnable diffusion term to better capture conditional variability and improve generalization. On the accountability side, we developed MCD-Antithetic, which combines Monte Carlo Dropout with variance-reduced (antithetic) SDE sampling and a nested decomposition of total uncertainty to enable sample-efficient OOD detection. Across cellular imaging (BBBC021, JUMP) and fMRI (Theory of Mind) benchmarks, SFM consistently improves generalization, while MCD-Antithetic yields strong, robust, and interpretable OOD detection performance under tight sampling budgets. These results provide a principled recipe for uncertainty-aware distribution-to-distribution generation.

Acknowledgement

This work was supported in part by ONR Grant N00014-22-1-2110, NSF Grant 2205084, and the Stanford Institute for Human-Centered Artificial Intelligence (HAI). EBF is a Biohub, San Francisco, Investigator. S.Y. is a Chan Zuckerberg Biohub — San Francisco Investigator.

References

- [1] Lemar Abdi, Amaan Valiuddin, Francisco Caetano, Christiaan Viviers, and Fons van der Sommen. Zero-shot image anomaly detection using generative foundation models. *arXiv preprint arXiv:2507.22692*, 2025. 3
- [2] Michael S Albergo, Nicholas M Boffi, and Eric Vanden-Eijnden. Stochastic interpolants: A unifying framework for flows and diffusions. *arXiv preprint arXiv:2303.08797*, 2023. 5
- [3] Fuat Arslan, Bilal Kabas, Onat Dalmaz, Muzaffer Ozbey, and Tolga Çukur. Self-consistent recursive diffusion bridge for medical image translation. *Medical Image Analysis*, 106:103747, 2025. 1, 3
- [4] Cosmin I Bercea, Benedikt Wiestler, Daniel Rueckert, and Julia A Schnabel. Diffusion models with implicit guidance for medical anomaly detection. In *International Conference on Medical Image Computing and Computer-Assisted Intervention*, pages 211–220. Springer, 2024. 3
- [5] Lucas Berry, Axel Brando, and David Meger. Shedding light on large generative networks: Estimating epistemic uncertainty in diffusion models. In *The 40th Conference on Uncertainty in Artificial Intelligence*, 2024. 3
- [6] Wolfgang Blau, Vinton G Cerf, Juan Enriquez, Joseph S Francisco, Urs Gasser, Mary L Gray, Mark Greaves, Barbara J Grosz, Kathleen Hall Jamieson, Gerald H Haug, et al. Protecting scientific integrity in an age of generative ai, 2024. 1
- [7] Peter D Caie, Rebecca E Walls, Alexandra Ingleston-Orme, Sandeep Daya, Tom Houslay, Rob Eagle, Mark E Roberts, and Neil O Carragher. High-content phenotypic profiling of drug response signatures across distinct cancer cells. *Molecular cancer therapeutics*, 9(6):1913–1926, 2010. 7, 14
- [8] Matthew Chan, Maria Molina, and Chris Metzler. Estimating epistemic and aleatoric uncertainty with a single model. *Advances in Neural Information Processing Systems*, 37:109845–109870, 2024. 3

- [9] Srinivas Niranj Chandrasekaran, Jeanelle Ackerman, Eric Alix, D Michael Ando, John Arevalo, Melissa Ben- nion, Nicolas Boisseau, Adriana Borowa, Justin D Boyd, Laurent Brino, et al. Jump cell painting dataset: morphological impact of 136,000 chemical and genetic perturbations. *BioRxiv*, pages 2023–03, 2023. 7, 14
- [10] Sungik Choi, Hankook Lee, Honglak Lee, and Moontae Lee. Projection regret: Reducing background bias for novelty detection via diffusion models. *Advances in Neural Information Processing Systems*, 36:19230–19245, 2023. 3
- [11] Valentin De Bortoli, James Thornton, Jeremy Heng, and Arnaud Doucet. Diffusion schrödinger bridge with applications to score-based generative modeling. *Advances in neural information processing systems*, 34:17695–17709, 2021. 3
- [12] Michele De Vita and Vasileios Belagiannis. Diffusion model guided sampling with pixel-wise aleatoric uncertainty estimation. In *2025 IEEE/CVF Winter Conference on Applications of Computer Vision (WACV)*, pages 3844–3854. IEEE, 2025. 3
- [13] Canberk Ekmekci and Mujdat Cetin. Conformalized generative bayesian imaging: An uncertainty quantification framework for computational imaging. *arXiv preprint arXiv:2504.07696*, 2025. 3
- [14] Berthy T Feng, Jamie Smith, Michael Rubinstein, Huiwen Chang, Katherine L Bouman, and William T Freeman. Score-based diffusion models as principled priors for inverse imaging. In *Proceedings of the IEEE/CVF International Conference on Computer Vision*, pages 10520–10531, 2023. 3
- [15] Gianni Franchi, Nacim Belkhir, Dat Nguyen Trong, Guoxuan Xia, and Andrea Pilzer. Towards understanding and quantifying uncertainty for text-to-image generation. In *Proceedings of the Computer Vision and Pattern Recognition Conference*, pages 8062–8072, 2025. 3
- [16] Yarin Gal and Zoubin Ghahramani. Dropout as a bayesian approximation: Representing model uncertainty in deep learning. In *international conference on machine learning*, pages 1050–1059. PMLR, 2016. 6
- [17] Silvio Galesso, Philipp Schröppel, Hssan Driss, and Thomas Brox. Diffusion for out-of-distribution detection on road scenes and beyond. In *European Conference on Computer Vision*, pages 110–126. Springer, 2024. 3
- [18] Ruiyuan Gao, Chenchen Zhao, Lanqing Hong, and Qiang Xu. Diffguard: Semantic mismatch-guided out-of-distribution detection using pre-trained diffusion models. In *Proceedings of the IEEE/CVF International Conference on Computer Vision*, pages 1579–1589, 2023. 3
- [19] Mark S Graham, Walter HL Pinaya, Petru-Daniel Tudosiu, Parashkev Nachev, Sebastien Ourselin, and Jorge Cardoso. Denoising diffusion models for out-of-distribution detection. In *Proceedings of the IEEE/CVF Conference on Computer Vision and Pattern Recognition*, pages 2948–2957, 2023. 3
- [20] Mark S Graham, Walter Hugo Lopez Pinaya, Paul Wright, Petru-Daniel Tudosiu, Yee H Mah, James T Teo, H Rolf Jäger, David Werring, Parashkev Nachev, Sebastien Ourselin, et al. Unsupervised 3d out-of-distribution detection with latent diffusion models. In *International Conference on Medical Image Computing and Computer-Assisted Intervention*, pages 446–456. Springer, 2023. 3
- [21] John Michael Hammersley and Keith William Morton. A new monte carlo technique: antithetic variates. In *Mathematical proceedings of the Cambridge philosophical society*, volume 52, pages 449–475. Cambridge University Press, 1956. 6
- [22] Alvin Heng, Harold Soh, et al. Out-of-distribution detection with a single unconditional diffusion model. *Advances in Neural Information Processing Systems*, 37:43952–43974, 2024. 3
- [23] Jonathan Ho and Tim Salimans. Classifier-free diffusion guidance. *arXiv preprint arXiv:2207.12598*, 2022. 4
- [24] Yue Huang, Chujie Gao, Siyuan Wu, Haoran Wang, Xiangqi Wang, Yujun Zhou, Yanbo Wang, Jiayi Ye, Jiawen Shi, Qihui Zhang, et al. On the trustworthiness of generative foundation models: Guideline, assessment, and perspective. *arXiv preprint arXiv:2502.14296*, 2025. 1
- [25] Metod Jazbec, Eliot Wong-Toi, Guoxuan Xia, Dan Zhang, Eric Nalisnick, and Stephan Mandt. Generative uncertainty in diffusion models. *arXiv preprint arXiv:2502.20946*, 2025. 3
- [26] Xuan Kan, Hejie Cui, Joshua Lukemire, Ying Guo, and Carl Yang. Fbnetgen: Task-aware gnn-based fmri analysis via functional brain network generation. In *International conference on medical imaging with deep learning*, pages 618–637. PMLR, 2022. 1, 3
- [27] Beomsu Kim, Gihyun Kwon, Kwanyoung Kim, and Jong Chul Ye. Unpaired image-to-image translation via neural schrödinger bridge. *arXiv preprint arXiv:2305.15086*, 2023. 3, 7
- [28] Eunwoo Kim, Un Yang, Cheol Lae Roh, and Stefano Ermon. Unsupervised anomaly detection using diffusion trend analysis for display inspection. *arXiv preprint arXiv:2407.09578*, 2024. 3

- [29] Polina Kirichenko, Pavel Izmailov, and Andrew G Wilson. Why normalizing flows fail to detect out-of-distribution data. *Advances in neural information processing systems*, 33:20578–20589, 2020. 8
- [30] Siqi Kou, Lei Gan, Dequan Wang, Chongxuan Li, and Zhijie Deng. Bayesdiff: Estimating pixel-wise uncertainty in diffusion via bayesian inference. *arXiv preprint arXiv:2310.11142*, 2023. 3, 7
- [31] Junbeom Kwon, Jungwoo Seo, Heehwan Wang, Taesup Moon, Shinjae Yoo, and Jiok Cha. Predicting task-related brain activity from resting-state brain dynamics with fmri transformer. *Imaging Neuroscience*, 3:imag_a.00440, 2025. 1, 3
- [32] Yunxiang Li, Hua-Chieh Shao, Xiao Liang, Liyuan Chen, Ruiqi Li, Steve Jiang, Jing Wang, and You Zhang. Zero-shot medical image translation via frequency-guided diffusion models. *IEEE transactions on medical imaging*, 43(3):980–993, 2023. 1, 3
- [33] Jasper Linmans, Gabriel Raya, Jeroen van der Laak, and Geert Litjens. Diffusion models for out-of-distribution detection in digital pathology. *Medical Image Analysis*, 93:103088, 2024. 3
- [34] Yaron Lipman, Ricky TQ Chen, Heli Ben-Hamu, Maximilian Nickel, and Matt Le. Flow matching for generative modeling. *arXiv preprint arXiv:2210.02747*, 2022. 2, 3
- [35] Yaron Lipman, Marton Havasi, Peter Holderrieth, Neta Shaul, Matt Le, Brian Karrer, Ricky TQ Chen, David Lopez-Paz, Heli Ben-Hamu, and Itai Gat. Flow matching guide and code. *arXiv preprint arXiv:2412.06264*, 2024. 3
- [36] Xingchao Liu, Chengyue Gong, and Qiang Liu. Flow straight and fast: Learning to generate and transfer data with rectified flow. *arXiv preprint arXiv:2209.03003*, 2022. 4
- [37] Zhenzhen Liu, Jin Peng Zhou, Yufan Wang, and Kilian Q Weinberger. Unsupervised out-of-distribution detection with diffusion inpainting. In *International Conference on Machine Learning*, pages 22528–22538. PMLR, 2023. 3
- [38] Wesley J Maddox, Pavel Izmailov, Timur Garipov, Dmitry P Vetrov, and Andrew Gordon Wilson. A simple baseline for bayesian uncertainty in deep learning. *Advances in neural information processing systems*, 32, 2019. 7
- [39] Chenlin Meng, Yutong He, Yang Song, Jiaming Song, Jiajun Wu, Jun-Yan Zhu, and Stefano Ermon. Sdedit: Guided image synthesis and editing with stochastic differential equations. *arXiv preprint arXiv:2108.01073*, 2021. 7
- [40] Alessandro Palma, Fabian J Theis, and Mohammad Lotfollahi. Predicting cell morphological responses to perturbations using generative modeling. *Nature Communications*, 16(1):505, 2025. 8
- [41] Taesung Park, Alexei A Efros, Richard Zhang, and Jun-Yan Zhu. Contrastive learning for unpaired image-to-image translation. In *European conference on computer vision*, pages 319–345. Springer, 2020. 3
- [42] Hilary Richardson, Grace Lisandrelli, Alexa Riobueno-Naylor, and Rebecca Saxe. Development of the social brain from age three to twelve years. *Nature communications*, 9(1):1027, 2018. 7, 15
- [43] Yuyang Shi, Valentin De Bortoli, Andrew Campbell, and Arnaud Doucet. Diffusion schrödinger bridge matching. *Advances in Neural Information Processing Systems*, 36:62183–62223, 2023. 3
- [44] Shirin Shoushtari, Yi Wang, Xiao Shi, M Salman Asif, and Ulugbek S Kamilov. Eigenscore: Ood detection using covariance in diffusion models. *arXiv preprint arXiv:2510.07206*, 2025. 3
- [45] Yang Song, Jascha Sohl-Dickstein, Diederik P Kingma, Abhishek Kumar, Stefano Ermon, and Ben Poole. Score-based generative modeling through stochastic differential equations. *arXiv preprint arXiv:2011.13456*, 2020. 5
- [46] Shiye Su, Yuhui Zhang, Linqi Zhou, Rajesh Ranganath, and Serena Yeung-Levy. Three forms of stochastic injection for improved distribution-to-distribution generative modeling. *arXiv preprint arXiv:2510.06634*, 2025. 3
- [47] Jacopo Teneggi, Matthew Tivnan, Web Stayman, and Jeremias Sulam. How to trust your diffusion model: A convex optimization approach to conformal risk control. In *International Conference on Machine Learning*, pages 33940–33960. PMLR, 2023. 3
- [48] Zihui Wu, Yu Sun, Yifan Chen, Bingliang Zhang, Yisong Yue, and Katherine Bouman. Principled probabilistic imaging using diffusion models as plug-and-play priors. *Advances in Neural Information Processing Systems*, 37:118389–118427, 2024. 3
- [49] Yutong Xie and Quanzheng Li. Measurement-conditioned denoising diffusion probabilistic model for under-sampled medical image reconstruction. In *International Conference on Medical Image Computing and Computer-Assisted Intervention*, pages 655–664. Springer, 2022. 3

- [50] Hui Zhang, Zheng Wang, Dan Zeng, Zuxuan Wu, and Yu-Gang Jiang. Diffusionad: Norm-guided one-step denoising diffusion for anomaly detection. *IEEE Transactions on Pattern Analysis and Machine Intelligence*, 2025. 3
- [51] Lily Zhang, Mark Goldstein, and Rajesh Ranganath. Understanding failures in out-of-distribution detection with deep generative models. In *International Conference on Machine Learning*, pages 12427–12436. PMLR, 2021. 8
- [52] Yuhui Zhang, Yuchang Su, Chenyu Wang, Tianhong Li, Zoe Wefers, Jeffrey Nirschl, James Burgess, Daisy Ding, Alejandro Lozano, Emma Lundberg, et al. Cellflux: Simulating cellular morphology changes via flow matching. *arXiv preprint arXiv:2502.09775*, 2025. 1, 2, 3, 4, 7, 8
- [53] Qinqing Zheng, Matt Le, Neta Shaul, Yaron Lipman, Aditya Grover, and Ricky TQ Chen. Guided flows for generative modeling and decision making. *arXiv preprint arXiv:2311.13443*, 2023. 4
- [54] Linqi Zhou, Aaron Lou, Samar Khanna, and Stefano Ermon. Denoising diffusion bridge models. *arXiv preprint arXiv:2309.16948*, 2023. 3
- [55] Jun-Yan Zhu, Taesung Park, Phillip Isola, and Alexei A Efros. Unpaired image-to-image translation using cycle-consistent adversarial networks. In *Proceedings of the IEEE international conference on computer vision*, pages 2223–2232, 2017. 3

A Proof of Proposition 4.1

Proof. We prove that the MAP estimate provides a good approximation to the expected aleatoric variance under concentrated posterior conditions.

Setup. Let $V(\theta, \phi) := \text{Var}(\mathbf{x}_1 | \mathbf{x}_0, c, \theta, \phi)$ denote the conditional variance as a function of parameters. Under the Laplace approximation, we have $p(\theta, \phi | \mathcal{D}) \approx \mathcal{N}((\hat{\theta}, \hat{\phi}), \mathbf{H}^{-1})$, where $(\hat{\theta}, \hat{\phi})$ is the MAP estimate and \mathbf{H} is the Hessian of the negative log-posterior at the MAP.

Step 1: Apply Lipschitz continuity. By the triangle inequality and Lipschitz continuity of V :

$$\begin{aligned} & \left| \mathbb{E}_{p(\theta, \phi | \mathcal{D})} [V(\theta, \phi)] - V(\hat{\theta}, \hat{\phi}) \right| \\ &= \left| \mathbb{E}_{(\theta, \phi) \sim \mathcal{N}((\hat{\theta}, \hat{\phi}), \mathbf{H}^{-1})} [V(\theta, \phi) - V(\hat{\theta}, \hat{\phi})] \right| \\ &\leq \mathbb{E}_{(\theta, \phi) \sim \mathcal{N}((\hat{\theta}, \hat{\phi}), \mathbf{H}^{-1})} [|V(\theta, \phi) - V(\hat{\theta}, \hat{\phi})|] \\ &\leq L \cdot \mathbb{E}_{(\theta, \phi) \sim \mathcal{N}((\hat{\theta}, \hat{\phi}), \mathbf{H}^{-1})} [\|(\theta, \phi) - (\hat{\theta}, \hat{\phi})\|_2], \end{aligned} \quad (25)$$

where the last inequality uses the L -Lipschitz property: $|V(\theta, \phi) - V(\theta', \phi')| \leq L \|(\theta, \phi) - (\theta', \phi')\|_2$.

Step 2: Bound the expected deviation. Let $\delta := (\theta, \phi) - (\hat{\theta}, \hat{\phi}) \sim \mathcal{N}(\mathbf{0}, \mathbf{H}^{-1})$ denote the parameter deviation from the MAP. By Jensen's inequality (since $\|\cdot\|_2$ is convex):

$$\mathbb{E}[\|\delta\|_2] = \mathbb{E} \left[\sqrt{\sum_{i=1}^d \delta_i^2} \right] \leq \sqrt{\mathbb{E} \left[\sum_{i=1}^d \delta_i^2 \right]} = \sqrt{\text{tr}(\mathbf{H}^{-1})}, \quad (26)$$

where $d = \dim(\theta, \phi)$ is the total parameter dimension.

Step 3: Apply the operator norm bound. Using the relationship between trace and operator norm:

$$\text{tr}(\mathbf{H}^{-1}) = \sum_{i=1}^d \lambda_i(\mathbf{H}^{-1}) \leq d \cdot \max_i \lambda_i(\mathbf{H}^{-1}) = d \cdot \|\mathbf{H}^{-1}\|_{\text{op}}, \quad (27)$$

where $\lambda_i(\mathbf{H}^{-1})$ are the eigenvalues of \mathbf{H}^{-1} and $\|\mathbf{H}^{-1}\|_{\text{op}}$ is the operator norm.

Step 4: Combine the bounds. By assumption, $\|\mathbf{H}^{-1}\|_{\text{op}} \leq \epsilon^2$. Therefore:

$$\mathbb{E}[\|\delta\|_2] \leq \sqrt{\text{tr}(\mathbf{H}^{-1})} \leq \sqrt{d \cdot \|\mathbf{H}^{-1}\|_{\text{op}}} \leq \sqrt{d \cdot \epsilon^2} = \epsilon \sqrt{d}. \quad (28)$$

Step 5: Final bound. Combining Steps 1 and 4:

$$\left| \mathbb{E}_{p(\theta, \phi | \mathcal{D})} [V(\theta, \phi)] - V(\hat{\theta}, \hat{\phi}) \right| \leq L \cdot \mathbb{E}[\|\delta\|_2] \leq L \epsilon \sqrt{d}. \quad (29)$$

□

B Dataset and OOD Scenario Details

Cell Imaging Datasets. **BBBC021** The BBBC021v1 dataset [7] from the Broad Bioimage Benchmark Collection is a benchmark for image-based phenotypic profiling of chemical perturbations in MCF-7 breast cancer cells. It contains 97,504 fluorescent microscopy images captured from cells treated with 113 small molecules at eight concentrations, targeting diverse cellular mechanisms including actin disruption, Aurora kinase inhibition, and microtubule stabilization. Each image provides multi-channel fluorescence for DNA, F-actin, and beta-tubulin, enabling detailed morphological analysis.

JUMP The JUMP dataset [9] is the most comprehensive image-based profiling resource to date, integrating both genetic and chemical perturbations. It comprises approximately 3 million images capturing phenotypic responses of 75 million single cells to genetic knockouts (CRISPR/ORF) and chemical treatments. The dataset includes two cell types: U2OS and A549. We use A549 cells for model training and U2OS cells for OOD evaluation. For our experiments, we use a subset of 72,000 images and focus exclusively on chemical perturbations.

Dataset	BBBC	BBBC	JUMP	JUMP	fMRI
OOD Case	Unseen Pert.	Intensity Shift	Unseen Cell Lines	Unseen Plates	Low ToM
# Channels	3	3	5	5	1
# Images	98K	98K	72K	72K	12K
Dist Shift	Extreme	High	Medium	Low	-

Table 4: Summary of Datasets and OOD Scenarios.

fMRI Dataset. We use the ds000228-1.1.1 dataset [42] containing MRI data of 3-12 year old children viewing a Pixar animated film. The task is to transform brain states from resting baseline (TRs 1-10, 20 seconds) to Theory of Mind (ToM) activation (7 events totaling 25 TRs, 50 seconds). We focus on slices 13-16 (4 middle brain slices capturing ToM-responsive regions: temporoparietal junction and medial prefrontal cortex), with each slice as a 64×64 grayscale image. The dataset includes 122 children categorized by False Belief performance: PASS group (84 subjects, mean ToM score: 0.883±0.102, age: 7.6±2.2 years) as in-domain, and INC+FAIL groups (38 subjects, mean ToM score: 0.537±0.148, age: 4.7±1.0 years) as out-of-distribution. Each subject contributes 40 rest images and 100 ToM images. The training set contains 9,712 images from PASS subjects, test ID set contains 2,048 randomly selected PASS images, and test OOD set contains 2,048 randomly selected INC+FAIL images, all normalized per slice.

C Implementation Details

Filtering Strategy for OOD Detection. To ensure the reliability of our OOD benchmarks, we filter out ambiguous samples that may not represent true in-distribution (ID) or out-of-distribution (OOD) behavior. For BBBC021, we compute the feature-space distance between model predictions and randomly paired ground truth treatment images using a pretrained mode-of-action classifier. For JUMP, we use the Structural Similarity Index Measure (SSIM) as the distance metric. We apply thresholds based on the distances calculated across the dataset. Specifically, we remove ID samples with distances greater than $\mu - 0.5\sigma$ (potentially poor generations) and remove OOD samples with distances smaller than $\mu + 0.5\sigma$ (samples that appear misleadingly in-distribution), where μ and σ denote the mean and standard deviation of the distance metric, respectively.

D Additional Experimental Results

D.1 Visualizing SFM Generalization

Figure 4, 5, 6, and 7 show additional examples of generated images from different methods on BBBC021 and JUMP under various OOD scenarios, compared with the source images and the ground truth target images.

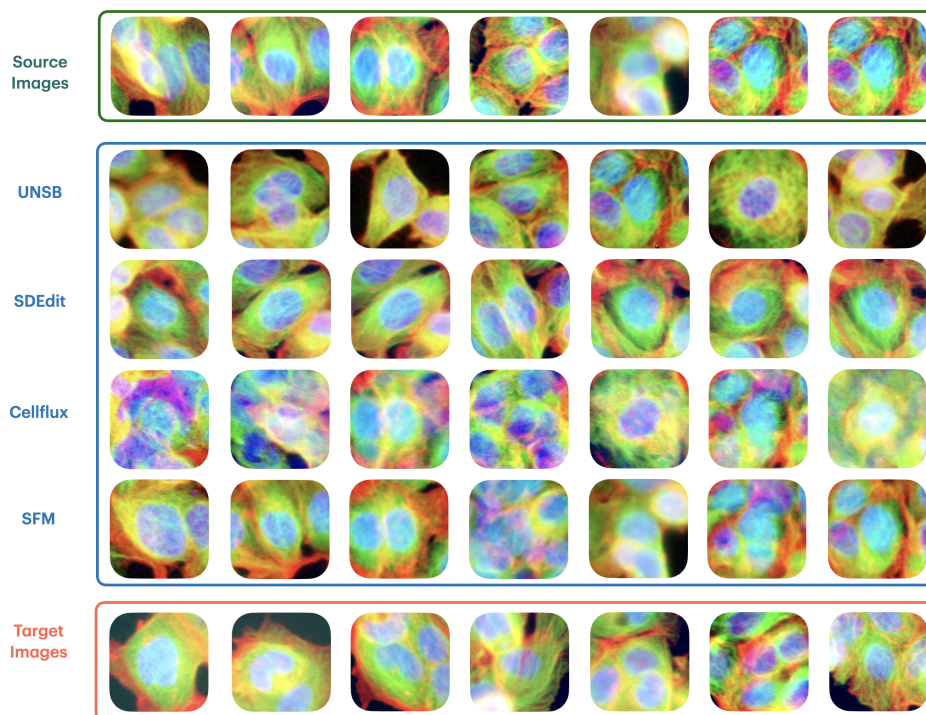


Figure 4: Examples of generated images from different methods on BBBC021 under Unseen Pert. OOD scenario, compared with the source images and the ground truth target images.

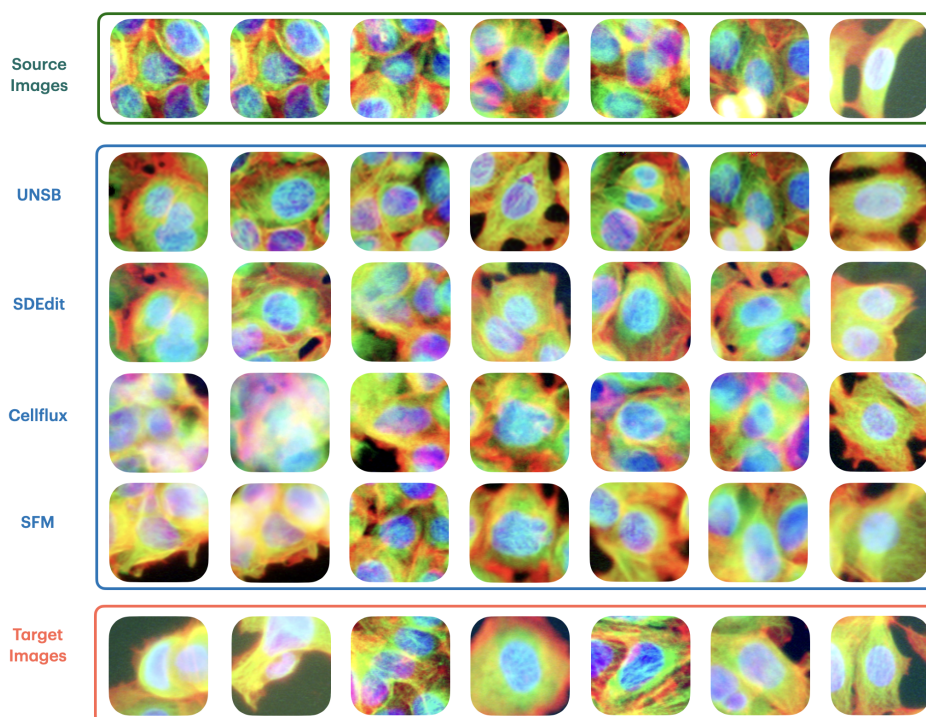


Figure 5: Examples of generated images from different methods on BBBC021 under Intensity Shift OOD scenario, compared with the source images and the ground truth target images.

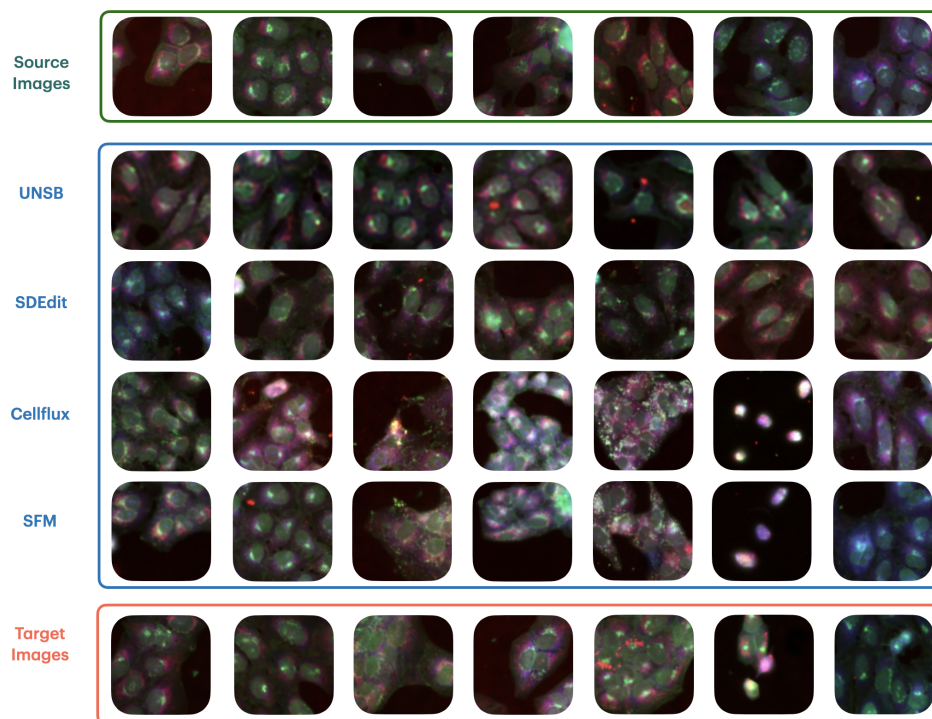


Figure 6: Examples of generated images from different methods on JUMP under Unseen Cell Lines OOD scenario, compared with the source images and the ground truth target images.

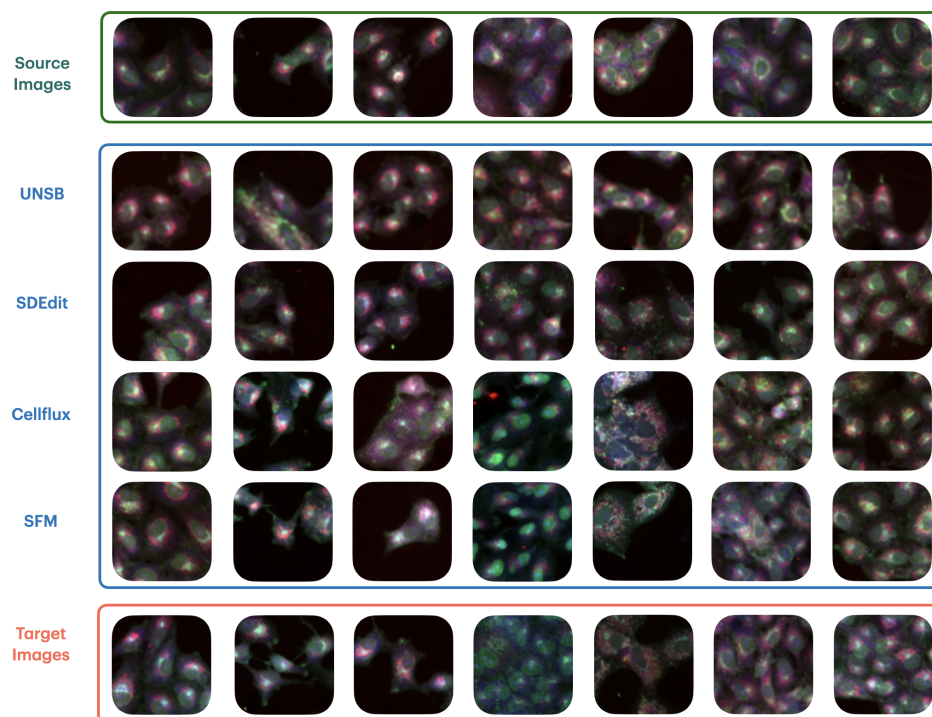


Figure 7: Examples of generated images from different methods on JUMP under Unseen Plates OOD scenario, compared with the source images and the ground truth target images.